Received: 5 February 2019 | Revised: 18 June 2019 | Accepted: 11 December 2019
DOI: 10.1002/we.2472

WILEY

RESEARCH ARTICLE

Proposals for a practical calibration method for mechanical torque measurement on the wind turbine drive train under test on a test bench

Hongkun Zhang[1] | Jan Wenske[1] | Andreas Reuter[2] | Mohsen Neshati[1]

[1]Fraunhofer Institute for Wind Energy Systems IWES, Bremerhaven, Germany
[2]Institut für Windenergiesysteme, Leibniz Universität Hannover, Hannover, Germany

Correspondence
Hongkun Zhang, Fraunhofer Institute for Wind Energy Systems IWES. Am Luneort 100, 27572 Bremerhaven, Germany.
Email: hongkun.zhang@iwes.fraunhofer.de

Abstract

The mechanical torque input into the wind turbine drive train is a very useful measurement for tests performed on a test bench. To ensure the accuracy and the reliability, an accurate calibration of the torque measurement must be carried out and repeated within a certain period of time. However, owing to the high torque level and large structure size, such a calibration is both expensive and time consuming. To overcome this challenge, a new calibration method is proposed here. The method is based on the electrical power measurement, where a high level of accuracy is much easier to achieve. With the help of a special test process, a relationship between the torque-measuring signal and the electrical power can be established. The process comprises two tests with the drive train running in different operating modes. The calibration is possible by carrying out the same test process on several different torque levels. Detailed uncertainty analysis of the method is presented, whereby the uncertainty can be calculated by means of matrix operation and also numerically. As a demonstration, the implementation of the method on a test bench drive train that contains two 5-MW motors in tandem with the motors operating in a back-to-back configuration is also presented. Finally, some variations on the method and possible ways of achieving better accuracy are discussed.

KEYWORDS

drive train, efficiency, test bench, torque calibration, torque measurement, wind turbine

1 | INTRODUCTION

The mechanical torque plays a very important role in the power transmission of wind turbines, transferring the mechanical power gained by the rotor all the way to the generator. Although due to certain restrictions the mechanical torque measurement (referred to simply as the "torque" below) is still not widely used in the everyday operation of wind turbines, it is indeed always an interesting variable for turbine tests both in a laboratory environment and in the field. Torque measurement is vital for the determination of the drive train efficiency, as well as the aerodynamic efficiency of the rotor. The enormous pressure to reduce costs in the wind energy industry makes efficiency a key parameter of the turbines on the market. Additionally, the level and variation of the input torque also have a strong influence on the fatigue damage of the components in the drive train, especially the gearbox.

Multi-MW wind turbines have one of the highest torque levels found in modern industries, along with hydro power and the shipbuilding, for example. For newer wind turbines with high rated power, the rated torque can be close to 10 MN·m, while the extreme torque is even higher. A calibration traceable to a national or international standard at this level is not possible at present, since the largest such calibration capacity available anywhere in the world is only 1.1 MN·m,[1] which is owned by the German national metrology institute PTB in Braunschweig. The governing calibration standard is the German DIN 51309 standard.[2] A new torque standard machine with a capacity of 5 MN·m is under development at the PTB.[3] Until adequate calibration capacity becomes available, the torque measurement can only be partially calibrated. Measurement behaviour beyond that has to be extrapolated.[4] Using this concept, the PTB has developed a 5-MN·m reference torque transducer

The peer review history for this article is available at https://publons.com/publon/10.1002/we.2472

(also known as "torque transfer standard").[5,6] It is intended to be a movable reference torque measurement, which can be used to calibrate other torque-measuring devices, for example on a wind turbine test bench. The PTB 1.1-MW torque standard machine has a relative uncertainty of 0.1 %.[7] The partially calibrated and extrapolated 5-MN·m torque transfer standard (TTS) has been found to have a relative uncertainty of 0.15 %.[5] This level of torque accuracy would be more than sufficient for the efficiency determination of the drive train. However, in order to achieve this accuracy in the test, a state-of-the-art torque transducer similar to the PTB 5-MN·m TTS (or the TTS itself) has to be installed directly in front of the drive train. Since the design, manufacture, and calibration of such torque transducers require high levels of professionalism, and also because each transducer has to be individually customized for the specific application, the cost of such transducers can be a big challenge for industrial use.

As a fundamental variable, torque measurement is instrumented in almost all the nacelle and drive-train test benches for wind turbines. However, there is no standard method for torque measurement. The solution for the measurement is mostly individually designed or specified for each of the test benches. Some discussions about the different methods used on the nacelle test benches are given in the work of Foyer et al.[6]

For test benches that apply 6-DOF (degree of freedom) loads, the torque-measuring device is usually not located directly between the test bench and the turbine nacelle. Instead, in order to reduce the impact of the non-torque loads and protect the torque transducer against the shocks, the inherent torque-measuring devices of such test benches are often located behind the load application unit (LAU) that applies for example the bending moment. As a result, the friction torque of the LAU can introduce a major uncertainty to the input torque for the turbine, especially given that the friction torque is also highly temperature and load dependent. Research undertaken by Kock et al[8] has studied the friction behaviours of a specific LAU system on a 4-MW test bench,[9] aiming to quantify the friction torque and the uncertainty introduced by the LAU system. To measure the input torque to the turbine directly, the torque transducer needs to be very robust, in order to withstand the large non-torque loads. One possible way is to use the shaft adapter between the test bench and the nacelle as a torque-measuring device. Certain strain gauge connections can be applied on the cylindrical adapter to measure the torque-introduced strain on the adapter. A calibration of enough accuracy is then necessary in order to convert the strain signal into torque.

For simpler test benches that apply only the torque, for example, the common end-of-line test benches of the turbine manufacturer, the accompanying non-torque loads are not as critical as above. In this case, torque measurement with professional torque transducers would be possible, but measuring with strain gauges on the adapter or connection shaft is still very attractive with lower cost of both funding and time.

On both types of test benches, accurate and regular calibrations are vital for the torque measurement where the accuracy is important, for example, to determine the drive-train efficiency. However, the high cost and great effort required for the calibration often make it impossible to achieve the desired high accuracy. Therefore, it makes good sense to seek a calibration process that is cost effective, practical to perform, and easy to repeat. Even for those applications where an accurate torque measurement is not necessary, for example when an uncertainty below 5 % is sufficient, such a calibration process is also an important means of validation.

This paper proposes a new calibration method that establishes a relationship between the torque and the electrical power, so that the torque measurement is indirectly calibrated through the electrical measurement. The relationship is determined through a series of tests whereby the test bench and the turbine nacelle take turns to drive and generate power. Because no additional structural reconfigurations and only limited instrumentation are needed for carrying out the calibration, the method has a clear advantage in time and cost perspectives. Due to a parameter estimation adopted in the process, the method cannot be categorised as traceable calibration, which is strictly traced back to the national or international standards with known uncertainty. But for easier understanding, the term ‘‘calibration’’ is still used in this paper to describe the process of determining the linear relationship between the measured raw signal and the torque. As a countermeasure to the estimation, a detailed analysis of the uncertainty budget related with the method is presented in this paper.

2 | TEST PROCESS

In the previous study, a test process was proposed to determine the drive train efficiency with limited accuracy of the torque measurement.[10,11] A further study has shown that the same test process can also be used for the calibration of the torque measurement. A relationship between the torque and the power measurement can be obtained through the test.

Two tests are necessary for the process, which are named test A and test B, respectively. The layout and the configuration of the tests are illustrated in Figure 1, where the power losses through the drive train are demonstrated using the level change of the power curves. In the figure, $P_{mech.A}$ and $P_{mech.B}$ are the mechanical powers at the measuring point for test A and test B, while $P_{elec.A}$ and $P_{elec.B}$ are the corresponding electrical powers. Similarly, T_A and T_B denote the mechanical torques for the two tests, while ω_A and ω_B represent the speeds of rotation. Torque measurement is realised on the shaft adapter between the test bench and the nacelle. Electrical power is measured between the turbine generator and the converter. Additionally, position and rotational speed of the shaft are also measured by the incremental or absolute encoder near the shaft adapter.

- In test A, the test bench and the turbine nacelle both operate in their normal mode. The test bench drives the nacelle running at a specific operating point. A warm-up operation should be carried out prior to the test in order to achieve stable temperature conditions for the components that influence the transmission and power conversion efficiency of the nacelle. The test should be run for a period of time, so that influences from the non-torque loads and the structural dynamics can be well compensated in the mean measurement value.
- In test B, the power flows in the direction opposite to that in test A. The nacelle operates in motor mode while the test bench acts as a generator. The nacelle drives the whole set-up so it is running at the same speed but in the direction opposite to that in test A. The measured

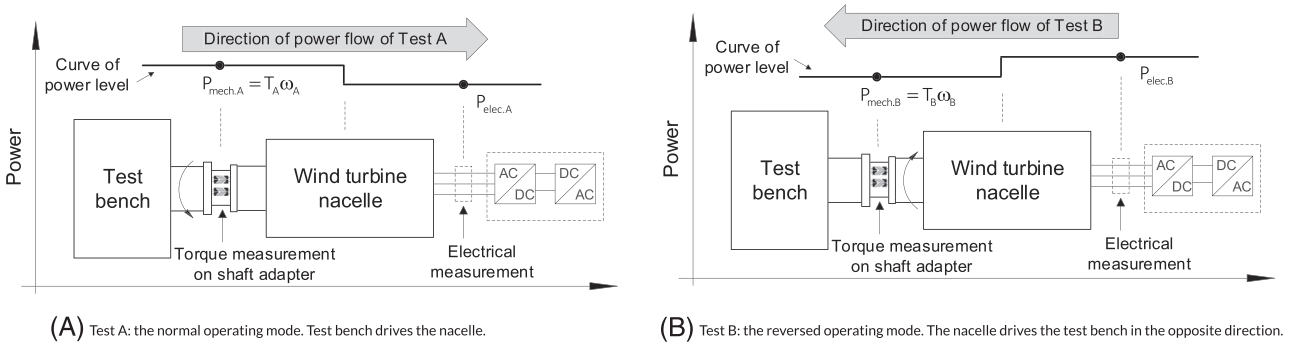

(A) Test A: the normal operating mode. Test bench drives the nacelle.

(B) Test B: the reversed operating mode. The nacelle drives the test bench in the opposite direction.

FIGURE 1 Layout and power loss demonstration of test A and test B

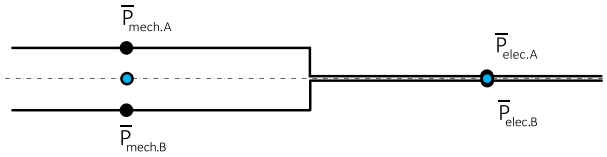

FIGURE 2 Levels of mechanical and electrical powers in test A and test B [Colour figure can be viewed at wileyonlinelibrary.com]

electrical power input to the nacelle generator should be carefully tuned to be as close as possible to the output power that is measured during test A. The test should also run for a similar time length as in test A.

For comparison, the input and output power levels of test A and test B can be plotted together as shown in Figure 2, where $\bar{P}_{mech.A}$ and $\bar{P}_{mech.B}$ are the mean values of the mechanical power in test A and test B, respectively, and $\bar{P}_{elec.A}$ and $\bar{P}_{elec.B}$ represent the mean values of the electrical power. It is worth emphasising that these four variables are the theoretical true values. The rotational speed is controlled to be stable throughout each test; therefore, the kinetic energy of the drive train inertia does not play a role in the equilibrium of the mean powers over a period of time.

The mean power loss in each of the tests can be expressed by definition as the difference between the input and output mean powers. This is shown in Equation (1), where $\bar{P}_{loss.A}$ and $\bar{P}_{loss.B}$ denote the mean value of the power loss in test A and test B, respectively. As the equation is expressed by the definition, $\bar{P}_{loss.A}$ and $\bar{P}_{loss.B}$ are also the true values without any uncertainty.

$$\begin{cases} \bar{P}_{loss.A} = \bar{P}_{mech.A} - \bar{P}_{elec.A} \\ \bar{P}_{loss.B} = \bar{P}_{elec.B} - \bar{P}_{mech.B}. \end{cases} \tag{1}$$

The factor k is introduced as the relationship between $\bar{P}_{loss.A}$ and $\bar{P}_{loss.B}$, as expressed in Equation (2). The equation can be further transformed into the expression in Equation (3), with the relationship from Equation (1).

$$\bar{P}_{loss.A} = k\bar{P}_{loss.B}, \tag{2}$$

$$\bar{P}_{mech.A} + k\bar{P}_{mech.B} = \bar{P}_{elec.A} + k\bar{P}_{elec.B}. \tag{3}$$

Other than drawing the relationship between the mechanical and electrical powers through the absolute drive train efficiency, Equation (3) forms the relationship based on the distribution of total power loss, which is depicted through a dash line in Figure 2. This is also the basis of the torque calibration method proposed in the present paper.

3 | METHOD OF TORQUE CALIBRATION

The mean values of the mechanical power $\bar{P}_{mech.A}$ and $\bar{P}_{mech.B}$ can be expressed as the accumulated energy divided by the corresponding duration, where the accumulated energy is the integrated torque in the angle domain. As a result, Equation (3) can be expressed further as Equation (4). In this equation, T denotes the torque, t_A and t_B are the durations of test A and test B, respectively, θ_A and θ_B are the corresponding accumulated angle displacements in test A and test B. Since the angular position is the raw signal from the encoder, it is more accurate to determine the power with the help of angle domain integration. Although encoders are often used on a wind turbine for measuring the rotational speed, the speed is in fact a derivative of the original position signal. For better accuracy, θ_A and θ_B can be chosen as integer multiples of 2π, so that the influence of the non-torque loads can be better compensated with signal from integer number of revolutions.

$$\frac{\int_0^{\theta_A} T d\theta}{t_A} + k\frac{\int_0^{\theta_B} T d\theta}{t_B} = \bar{P}_{elec.A} + k\bar{P}_{elec.B}. \tag{4}$$

Replacing the theoretical true variables with the measured values, T and P_{elec} can be expressed as in Equation (5), where

- ε represents the measured raw signal from the the torque measurement channel. In many cases, the raw signal is the strain measured by the strain gauges. Depending on the measurement principle and the channel configuration, the raw signal can also be other variables.
- a and b are the sensitivity and offset parameters that define the linear relationship between the measured raw signal ε and the true torque T. Due to the non-linear behaviour of the measurement and external influences, the real relationship can be more complicated than the linear one defined by a and b. The discrepancy from the linear behaviour is attributed to a time-varying quantity $r(t)$, which also includes the repeatability error of the measurement, for example the error caused by temperature change and the noise from EMI (Electromagnetic Interference).
- $\tilde{P}_{elec}$ is the measured signal of the electrical power. c and d are the sensitivity and offset errors of the measurement with respect to the true electrical power P. Similar to the $r(t)$ in the torque measurement, $q(t)$ denotes here the non-linearity and the repeatability errors of the electrical power measurement.

$$\begin{cases} T = a\varepsilon + b + r(t) \\ P_{elec} = (1+c)\tilde{P}_{elec} + d + q(t). \end{cases} \tag{5}$$

Using the definitions in Equation (5), the mean torque values can be expressed as Equation (6), where $\bar{\omega}_A$ and $\bar{\omega}_B$ are the mean rotational speeds in test A and test B, respectively. For the mean rotational speed, no distinction is made here between the theoretical true value and the measured value. The high positional accuracy provided by the encoder and the relatively long test period make it possible that the error of the measured mean speed can be regarded as zero. The right-hand side of Equation (4) can be expressed as Equation (7), with $\bar{\tilde{P}}_{elec.A}$ and $\bar{\tilde{P}}_{elec.B}$ being the mean values of the measured electrical power in test A and test B.

Defining $R_A = \frac{1}{t_A}\int_0^{\theta_A} r(\theta)d\theta$, $R_B = \frac{1}{t_B}\int_0^{\theta_B} r(\theta)d\theta$, $Q_A = \frac{1}{t_A}\int_0^{t_A} q(t)dt$, and $Q_B = \frac{1}{t_B}\int_0^{t_B} q(t)dt$, Equation (4) can be transformed into Equation (8).

$$\begin{cases} \dfrac{\int_0^{\theta_A} Td\theta}{t_A} = \dfrac{a}{t_A}\displaystyle\int_0^{\theta_A} \varepsilon(\theta)d\theta + b\bar{\omega}_A + \frac{1}{t_A}\int_0^{\theta_A} r(\theta)d\theta \\ \dfrac{\int_0^{\theta_B} Td\theta}{t_B} = \dfrac{a}{t_B}\displaystyle\int_0^{\theta_B} \varepsilon(\theta)d\theta + b\bar{\omega}_B + \frac{1}{t_B}\int_0^{\theta_B} r(\theta)d\theta, \end{cases} \tag{6}$$

$$\bar{P}_{elec.A} + k\bar{P}_{elec.B} = (1+c)(\bar{\tilde{P}}_{elec.A} + k\bar{\tilde{P}}_{elec.B}) + d(1+k) + \frac{1}{t_A}\int_0^{t_A} q(t)dt + \frac{1}{t_B}\int_0^{t_B} q(t)dt, \tag{7}$$

$$a\left(\frac{\int_0^{\theta_A}\varepsilon d\theta}{t_A} + \frac{k\int_0^{\theta_B}\varepsilon d\theta}{t_B}\right) + b(\bar{\omega}_A + k\bar{\omega}_B) + R_A + R_B = (1+c)(\bar{\tilde{P}}_{elec} + k\bar{\tilde{P}}_{elec}) + d(1+k) + Q_A + Q_B. \tag{8}$$

Denoting X and Y as expressed in Equations (9) and (10), the relationship defined in Equation (4) can be expressed in a concise form shown in Equation (11). A very clear linear relationship is seen in this equation, with a and b being the sensitivity and offset parameters. In fact, the aim of the calibration is exactly this—to determine the values of a and b.

It is obvious here that the parameters a and b can be determined with at least two sets of X and Y values at different torque levels. This means the test procedure described in Section 2 should be carried out on several different torque levels. If more than two sets of values are available, a and b can be determined through linear fit using the least squares method.

$$X = \frac{\int_0^{\theta_A}\varepsilon d\theta}{t_A(\bar{\omega}_A + k\bar{\omega}_B)} + \frac{k\int_0^{\theta_B}\varepsilon d\theta}{t_B(\bar{\omega}_A + k\bar{\omega}_B)}, \tag{9}$$

$$Y = \frac{(1+c)(\bar{\tilde{P}}_{elec.A} + k\bar{\tilde{P}}_{elec.B}) + d(1+k) + Q_A + Q_B - R_A - R_B}{\bar{\omega}_A + k\bar{\omega}_B}, \tag{10}$$

$$aX + b = Y. \tag{11}$$

As can be seen in Equations (9) and (10), the X and Y values are expressions of the mechanical and electrical measurement as well as the factor k. Additionally, some error terms are also in the expression, including c, d, Q_A, Q_B, R_A, and R_B. The measured mechanical and electrical values are of course known for the calculation. The factor k must be determined through analysis to become a known value, denoted as $\hat{k}$, with the uncertainty taken into account. Note that the k factor is not necessarily estimated as 1. In the calibration process, the error terms in the expression do not play any part, but they will be taken as uncertainty contributions in the following uncertainty analysis.

$$\begin{cases} \tilde{X} = \dfrac{\int_0^{\theta_A}\varepsilon d\theta}{t_A(\bar{\omega}_A + \hat{k}\bar{\omega}_B)} + \dfrac{\hat{k}\int_0^{\theta_B}\varepsilon d\theta}{t_B(\bar{\omega}_A + \hat{k}\bar{\omega}_B)} \\ \tilde{Y} = \dfrac{\bar{\tilde{P}}_{elec.A} + \hat{k}\bar{\tilde{P}}_{elec.B}}{\bar{\omega}_A + \hat{k}\bar{\omega}_B}. \end{cases} \tag{12}$$

For the calibration, the $\tilde{X}$-$\tilde{Y}$ value sets can be used for determining the parameters a and b. $\tilde{X}$ and $\tilde{Y}$ are defined in Equation (12). All the terms in the expressions are known values, and therefore, the calibration can easily be carried out. Suppose the test process in Section 2 is carried out on N different torque levels (N≥2), the estimated values of a and b, denoted as â and $\hat{b}$, can be obtained through the linear fit,[12, p246] and the results can be expressed as Equations (13) and (14), where i is the index number of a certain torque level, $\tilde{X}_i$ and $\tilde{Y}_i$ are the corresponding values obtained on the basis of that test. Note that the estimated value $\hat{k}$ may be different for tests with different torque levels.

$$\hat{a} = \frac{N\sum_{i=1}^{N}\tilde{X}_i\tilde{Y}_i - \sum_{i=1}^{N}\tilde{X}_i\sum_{i=1}^{N}\tilde{Y}_i}{N\sum_{i=1}^{N}(\tilde{X}_i^2) - (\sum_{i=1}^{N}\tilde{X}_i)^2}, \tag{13}$$

$$\hat{b} = \frac{\sum_{i=1}^{N}(\tilde{X}_i^2)\sum_{i=1}^{N}\tilde{Y}_i - \sum_{i=1}^{N}\tilde{X}_i\sum_{i=1}^{N}(\tilde{X}_i\tilde{Y}_i)}{N\sum_{i=1}^{N}(\tilde{X}_i^2) - (\sum_{i=1}^{N}\tilde{X}_i)^2}. \tag{14}$$

With the â and $\hat{b}$ known, and taking the definition in Equation (5) as the basis, the estimated torque $\hat{T}$ can be calculated in Equation (15). The term $r(t)$ contributes to the uncertainty of the torque calculation.

$$\hat{T} = \hat{a}\varepsilon + \hat{b} + r(t). \tag{15}$$

With $r(t)$ being considered as a source of uncertainty, the expression can be simplified to Equation (16).

$$\hat{T} = \hat{a}\varepsilon + \hat{b}. \tag{16}$$

4 | UNCERTAINTY CONSIDERATIONS

As a result of the calibration process, the torque measurement can be expressed as a function of the estimated â, $\hat{b}$ and the measured raw signal ε. A time-varying variable $r(t)$ takes account of the repeatability error of the measured signal as well as the non-linearity error of the T-ε relationship. This situation is presented in Equation (15). The uncertainty in $\hat{T}$ is therefore dependent on â, $\hat{b}$, ε and $r(t)$.

The uncertainty of the measured torque is ultimately composed of two parts. One part originates from the raw measurement itself, the other from the calibration. The uncertainty in the raw measurement represents the quality of the measured raw signal, which is affected by the signal noise, non-linear and hysteresis behaviour, signal drift due to temperature change and humidity, as well as other possible factors that make the signal less repeatable. The uncertainty from the calibration indicates how accurately the sensitivity and offset parameters are derived from the calibration. This paper will focus on the calibration uncertainty. Although the raw measurement uncertainty is not of great interest here, it does exert an influence on the calibration uncertainty, because the raw signals have to be used in the calibration process. A better calibration cannot improve the quality of the raw measurement, but better raw signals can indeed produce a more accurate calibration.

4.1 | Uncertainty of the raw measurement

Since the variable ε is defined as the value of the raw measurement, the uncertainty of ε itself should be considered to be zero. As a result, the uncertainty of the torque measurement directly owing to the raw signal is attributed to $r(t)$, which is introduced in Equation (5) to represent all the error contributions that cause the measured signal ε to deviate from the ideal linear response to the true torque. The error contributions can be grouped into two categories, namely, the non-linear behaviour and the repeatability errors. The total uncertainty contributed by $r(t)$ is denoted here as $u_{T,r}$. It characterises the quality of the measuring channel.

The non-linearity of a measurement is strongly dependent on the principle used and the measurement chain. In the case of a strain gauge-based measurement, it depends on the material and structural non-linear behaviour of the part to which the strain gauges are applied, as well as the non-linearity of the Wheatstone bridge circuit.[13] Further, non-linearity comes also from the data acquisition (DAQ) system of the measurement.

The repeatability error of the measurement comes from a number of sources that cause the measurement to be time-varying. A common source is the background noise in the measured signal due to EMI and the thermal noise[14] in the strain gauge resistors. Creep effect of the material and temperature change both cause a signal drift in the measurement and therefore also contribute to the repeatability error. Another contributor is the so-called "cross-talk" effect, which means that the load in other directions exert an influence on the torque measurement. Despite the effort and common methods available for the compensation against cross-talk,[15] a satisfactory compensation is usually very difficult on a wind turbine.[16] Fortunately, in some cases, the transient value of the measurement is of less interest, for example, in a stable operation on the test bench. The torque can then be determined by the mean of a period of time, or more precisely the mean value of an integer number of revolutions. This will be the case for a torque calibration test process as mentioned in Sections 2 and 3.

4.2 | Uncertainty associated with the calibration

The parameters â and $\hat{b}$ are the results of the linear fit of a number of ($\tilde{X}_i$-$\tilde{Y}_i$) points in the X-Y plane. This is schematically illustrated in Figure 3, where four points are available. For each point, both $\tilde{X}_i$ and $\tilde{Y}_i$ have uncertainties. The uncertainties are presented in the form of error bars, with

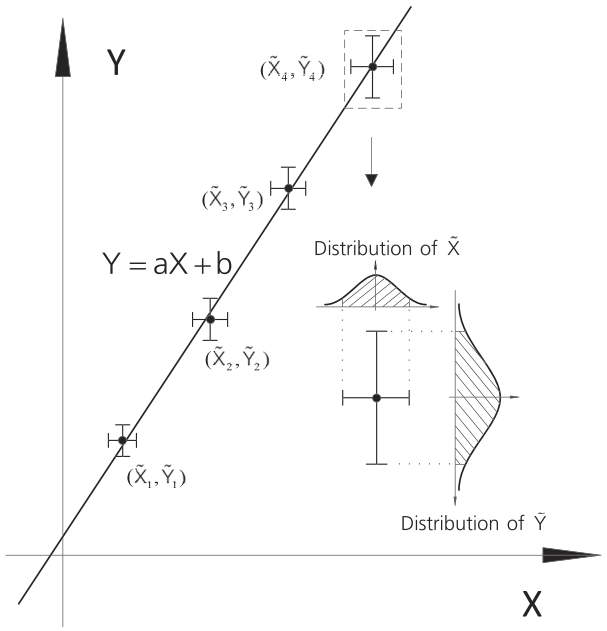

FIGURE 3 Linear fit in the X-Y plane

the corresponding estimated values $\tilde{X}_i$ and $\tilde{Y}_i$ located in the middle of the error bars. The length of the error bar represents the uncertainty of the corresponding variable, although this does not necessarily mean that the true value is located within the range defined by the bar. The probability distribution of the true value within and beyond the error bar can be of different types. The most common form is the normal distribution, as shown enlarged in the lower right part of Figure 3. Each individual uncertainty represented by the error bar makes a contribution to the uncertainty in â and $\hat{b}$ and hence the measured torque $\hat{T}$. Therefore, all the uncertainties of the $\tilde{X}_i$ and $\tilde{Y}_i$ values have to be considered in the uncertainty calculation for â, $\hat{b}$.

Furthermore, the uncertainty covariances of each two values also exert influence on the overall uncertainties of â, $\hat{b}$. These include the uncertainty covariance of each two different $\tilde{X}$ values, of each two different $\tilde{Y}$ values, and the uncertainty covariance of each $\tilde{X}$ and $\tilde{Y}$ combination. In fact, because the same k factor is used in the expression of both $\tilde{X}$ and $\tilde{Y}$, and also since the measurements on different torque levels are obtained from the same measurement chain, the covariances are of considerable significance. The standard uncertainty in $\hat{T}$ due to the linear fit parameters â and $\hat{b}$ (which are also the products of the calibration) is denoted in the following as $u_{T.cal}$.

The uncertainty $u_{T.cal}$ represents the uncertainty of the $(\hat{a}\varepsilon + \hat{b})$ part of Equation (15), where â and $\hat{b}$ are functions of N sets of $\tilde{X}_i$-$\tilde{Y}_i$ values. Following the principle of uncertainty propagation,[17] $u_{T.cal}$ can be determined,[12, p253] as expressed in Equation (17).

$$\begin{aligned} u_{T.cal}^2 = & \sum_{i=1}^{N}\left(\frac{\partial \hat{T}}{\partial \tilde{Y}_i}\right)^2 s_{\tilde{Y}_i}^2 + \sum_{i=1}^{N}\left(\frac{\partial \hat{T}}{\partial \tilde{X}_i}\right)^2 s_{\tilde{X}_i}^2 + \sum_{i=1}^{N}\left(\frac{\partial \hat{T}}{\partial \tilde{Y}_i}\right)^2 \sigma_{\tilde{Y}_i}^2 \\ & + 2\sum_{i=1}^{N-1}\sum_{k=i+1}^{N}\left(\frac{\partial \hat{T}}{\partial \tilde{Y}_i}\right)\left(\frac{\partial \hat{T}}{\partial \tilde{Y}_k}\right)\sigma_{\tilde{Y}_i\tilde{Y}_k} + \sum_{i=1}^{N}\left(\frac{\partial \hat{T}}{\partial \tilde{X}_i}\right)^2 \sigma_{\tilde{X}_i}^2 \\ & + 2\sum_{i=1}^{N-1}\sum_{k=i+1}^{N}\left(\frac{\partial \hat{T}}{\partial \tilde{X}_i}\right)\left(\frac{\partial \hat{T}}{\partial \tilde{X}_k}\right)\sigma_{\tilde{X}_i\tilde{X}_k} + 2\sum_{i=1}^{N}\sum_{k=1}^{N}\left(\frac{\partial \hat{T}}{\partial \tilde{X}_i}\right)\left(\frac{\partial \hat{T}}{\partial \tilde{Y}_k}\right)\sigma_{\tilde{X}_i\tilde{Y}_k} \end{aligned} \tag{17}$$

where $s_{\tilde{X}_i}$ and $s_{\tilde{Y}_i}$ are the random standard uncertainties in the variables $\tilde{X}_i$ and $\tilde{Y}_i$, respectively.

$\sigma_{\tilde{X}_i}$ and $\sigma_{\tilde{Y}_i}$ similarly denote the systematic standard uncertainty of $\tilde{X}_i$ and $\tilde{Y}_i$.

$\sigma_{\tilde{Y}_i\tilde{Y}_k}$, $\sigma_{\tilde{X}_i\tilde{X}_k}$ and $\sigma_{\tilde{X}_i\tilde{Y}_k}$ are the covariance estimators for the correlated systematic errors of the corresponding variables in the subscript.

Examining the equation, it is seen that most of the terms are very easy to obtain:

- The partial derivatives of $\frac{\partial \hat{T}}{\partial \tilde{X}_i}$ and $\frac{\partial \hat{T}}{\partial \tilde{Y}_i}$ can be estimated numerically on the basis of the finite difference method. According to Equations (13), (14), and (16), the estimated torque $\hat{T}$ can be explicitly expressed with the estimated $\tilde{X}$, $\tilde{Y}$ values and the measured signal ε, all of which are known or already determined.
- The random uncertainties $s_{\tilde{X}_i}$ and $s_{\tilde{Y}_i}$ refer to the uncertainty components which are independent and have no correlation with other components. Based on the definition of X and Y in Equations (9) and (10), the random uncertainty $s_{\tilde{X}_i}$ can be considered as zero, because the accuracy of the time and angle position measurements (and hence the mean speed as well) are very high, and as a result, their uncertainties are negligible. The value of $s_{\tilde{Y}_i}$ is mostly dependent on the random uncertainty of the electrical power measurement.
- The systematic uncertainties $\sigma_{\tilde{X}_i}$ and $\sigma_{\tilde{Y}_i}$ are introduced by systematic reasons and can therefore be related with the uncertainties from other measurements. For example, the uncertainty in the measured electrical power on a certain power level can be related to the uncertainty on

another power level or on the same level from another test. The values of $\sigma_{\tilde{X}_i}$ and $\sigma_{\tilde{Y}_i}$ are dependent on the uncertainties from the estimated $\hat{k}$ factor and the electrical power measurement.

- The effect of the correlations between the systematic uncertainties is quantified in the calculation with covariances $\sigma_{\tilde{Y}_i\tilde{Y}_k}$, $\sigma_{\tilde{X}_i\tilde{X}_k}$, and $\sigma_{\tilde{X}_i\tilde{Y}_k}$. The covariance can be further expressed as a function of two systematic uncertainties and the corresponding correlation coefficient between them,[17] as expressed in Equation (18). Therefore, the task of determining the covariances is converted to the determination of correlation coefficients.

$$\begin{cases} \sigma_{\tilde{X}_i\tilde{X}_k} = \sigma_{\tilde{X}_i}\sigma_{\tilde{X}_k} r_{\tilde{X}_i\tilde{X}_k} \\ \sigma_{\tilde{Y}_i\tilde{Y}_k} = \sigma_{\tilde{Y}_i}\sigma_{\tilde{Y}_k} r_{\tilde{Y}_i\tilde{Y}_k} \\ \sigma_{\tilde{X}_i\tilde{Y}_k} = \sigma_{\tilde{X}_i}\sigma_{\tilde{Y}_k} r_{\tilde{X}_i\tilde{Y}_k}. \end{cases} \tag{18}$$

Although Equation (17) appears complicated with the large number of terms, most of the terms are in fact the diagonal and cross entries of a $2N \times 2N$ matrix. Therefore, the equation is suitable for processing with matrix operations. One possible way of establishing such a matrix operation is discussed in this section.

Define a row vector $\boldsymbol{v}$ as the array of partial derivatives with respect to $\tilde{X}$ and $\tilde{Y}$ at different torque levels. The vector has $2N$ elements, and is expressed in Equation (19). Similarly, define σ as a row vector containing $\sigma_{\tilde{X}}$ and $\sigma_{\tilde{Y}}$ at different torque levels as expressed in Equation (20). Vector σ also has $2N$ elements. Based on $\boldsymbol{v}$ and σ, two $2N \times 2N$ matrices $(\boldsymbol{v}^{\mathrm{T}}\boldsymbol{v})$ and $(\sigma^{\mathrm{T}}\sigma)$ can be obtained by means of simple matrix operations. Each matrix contains all the possible products of two different elements from the corresponding vector (the cross entries of the matrix), as well as products of each vector element with itself (diagonal entries of the matrix). In matrix $(\sigma^{\mathrm{T}}\sigma)$, each entry is a product of two standard systematic uncertainties. According to Equation (18), this product can be converted to the covariance of the two uncertainties after being multiplied by the relevant correlation coefficient. Inserting this correlation coefficient into the corresponding position of another $2N \times 2N$ matrix and repeating this for all the entries allows matrix of correlation coefficients to be obtained. This new matrix is denoted here as $\boldsymbol{R}$.

$$\boldsymbol{v} = \left(\frac{\partial \hat{T}}{\partial \tilde{X}_1}, \ldots, \frac{\partial \hat{T}}{\partial \tilde{X}_N}, \frac{\partial \hat{T}}{\partial \tilde{Y}_1}, \ldots, \frac{\partial \hat{T}}{\partial \tilde{Y}_N} \right), \tag{19}$$

$$\sigma = \left(\sigma_{\tilde{X}_1}, \ldots, \sigma_{\tilde{X}_N}, \sigma_{\tilde{Y}_1}, \ldots, \sigma_{\tilde{Y}_N} \right). \tag{20}$$

The Hadamard product of matrix $(\boldsymbol{v}^{\mathrm{T}}\boldsymbol{v})$, $(\sigma^{\mathrm{T}}\sigma)$ and $\boldsymbol{R}$, denoted as $\boldsymbol{U}_{\boldsymbol{sys}}$ in Equation (21), contains all the systematic uncertainty components in $u^2_{T.cal}$ as expressed in Equation (17). A summation of all the entries of matrix $\mathbf{U}_{\mathbf{sys}}$ is easy to achieve in the calculation and can be expressed analytically as $\mathbf{e}\mathbf{U}_{\mathbf{sys}}\mathbf{e}^{\mathrm{T}}$, where $\boldsymbol{e}$ is a row vector with all elements being 1. Therefore, with the help of matrix operations, the expression of $u^2_{T.cal}$ in Equation (17) can be converted into a concise form shown in Equation (22).

$$\mathbf{U}_{sys} = (\boldsymbol{v}^{\mathrm{T}}\boldsymbol{v}) \circ (\sigma^{\mathrm{T}}\sigma) \circ \boldsymbol{R}, \tag{21}$$

$$u^2_{T.cal} = \sum_{i=1}^{N} \left(\frac{\partial \hat{T}}{\partial \tilde{Y}_i}\right)^2 s^2_{\tilde{Y}_i} + \sum_{i=1}^{N} \left(\frac{\partial \hat{T}}{\partial \tilde{X}_i}\right)^2 s^2_{\tilde{X}_i} + \boldsymbol{e}\boldsymbol{U}_{\boldsymbol{sys}}\boldsymbol{e}^{\mathrm{T}}. \tag{22}$$

In summary, the systematic uncertainty can be obtained using the two vectors $\boldsymbol{v}$ and σ, together with the correlation matrix $\boldsymbol{R}$. The calculation process is suitable for matrix operations, which can be effectively carried out with computer programmes or commercial mathematical software. While $\boldsymbol{v}$ and σ can be easily obtained through numerical calculation, the matrix $\boldsymbol{R}$ requires more analysis of the uncertainty source. Due to space limitation, the analysis is not discussed in detail in this paper. Nevertheless, the matrix $\boldsymbol{R}$ is not difficult to obtain as most of its entries are close or equal to zero or one.

5 | EXPERIMENT WITH THE METHOD ON A 10-MW NACELLE TEST BENCH

During a re-commissioning of the motors on the nacelle test bench "DyNaLab,"[18] the mechanical torque on the structure between the two tandem motors is needed for the validation of the electrical model of the motors, which is a basis of the motor controller. In order to measure the torque between the motors, strain gauges are applied to the intermediate shaft between the motors, and thus the measured signal from the strain gauges needs to be calibrated. One possible calibration method is the FEM analysis of the intermediate shaft, where the relationship between structure strain and torque can be established. However, the accuracy is considered insufficient due to the accumulated uncertainty from the strain measurement and the FEM analysis. Another method is to apply torque on one side of the drive train with a lift crane over a lever of known length. The problem with this method is the logistic expense and the difficulty to lock the drive train on the other side.

After evaluation of possible ways of calibration, the method proposed in this paper is considered to be the most convenient and accurate way of calibration. Additionally, the efficiencies of the motors at different operation points can be also determined as by-products. The method and test process are therefore carried out during the re-commissioning.

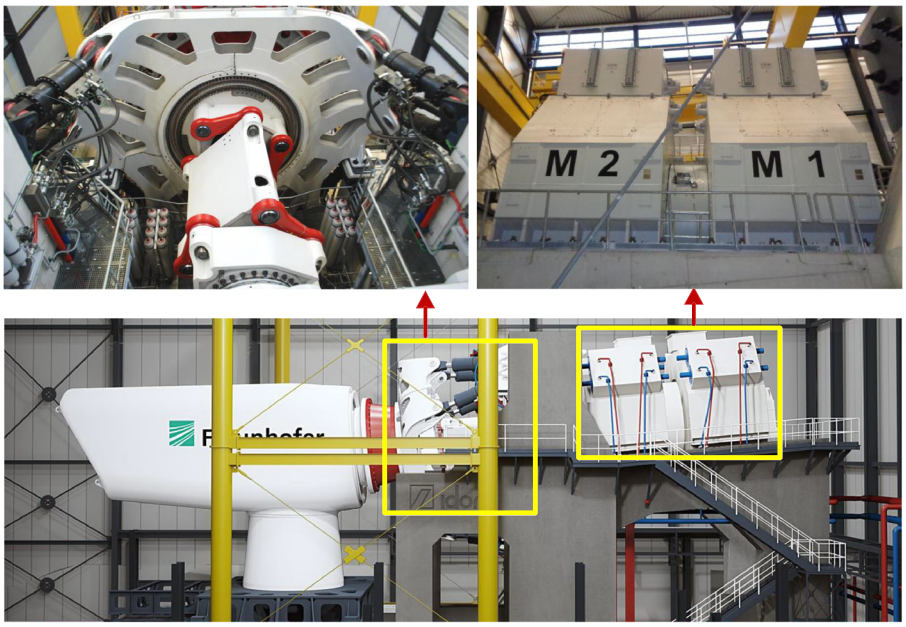

FIGURE 4 The 10 MW nacelle test bench "DyNaLab" at Fraunhofer IWES in Bremerhaven. Top left: the coupling and load application system (LAU) with a moment bearing. Top right: two tandem motors and the intermediate shaft. Bottom: overview of the test bench [Colour figure can be viewed at wileyonlinelibrary.com]

TABLE 1 Parameters per one motor

Motor Type	Rated power	Rated torque	Overload Torque	Rated speed	Speed range
Synchronous	5000 kW	4.3 $MN \cdot m$	6.5 $MN \cdot m$	11 rpm	2.5 - 25 rpm

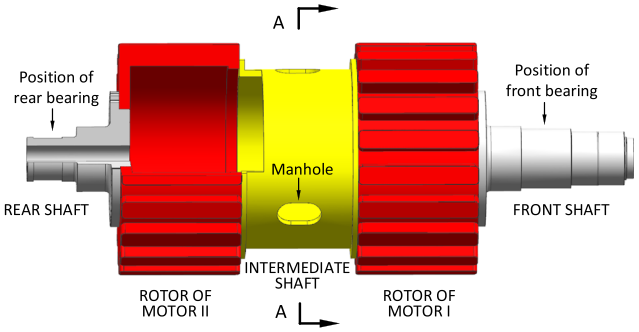

FIGURE 5 Drive train layout of the drive system [Colour figure can be viewed at wileyonlinelibrary.com]

The motors and the test bench "DyNaLab" are shown in Figure 4. Two motors are connected together in tandem by an intermediate shaft between them. The basic information about a single motor is listed in Table 1. In the normal operation, the two motors work together to provide the driving torque of the test bench. During the re-commissioning, the motors run in back-to-back mode instead. In application of the new method, motor I and motor II correspond to the test bench and the turbine, respectively, as described in Sections 2 and 3.

5.1 | Instrumentation of the measurement system

The drive train layout of the two motors is shown in Figure 5. The rotors are connected together and supported by two bearings on the front and rear shafts. The intermediate shaft as well as the rotors have a hollow structure. Three manholes are available on the intermediate shaft, which enable operations to be carried out inside the rotating part, for example, applying the strain gauges on the inner surface from inside the structure. Owing to the large diameter of the intermediate shaft, this has clear logistic advantages over applying the strain gauges on the outer surface.

The strain gauges and the instrumentation for the measurement are illustrated in detail with a cross-sectional sketch of the middle of the intermediate shaft in the A-A direction, as shown in Figure 6.

Three identical wheatstone strain gauge full bridges are applied at three different positions on the inner surface of the structure, labelled as 60°, 180°, and 300° in the figure. The positions are chosen to be as far away from the manholes as possible, which means that they are located at the mid-points between the manholes. This keeps the strain gauges away from the strain concentration and complexity at the vicinity of the manholes. The full bridges are applied so as to measure the local shear strain. Each full bridge is located at a single position, and therefore, the temperature difference within the full bridge is minimised. In order to compensate the strain component that is introduced by the shear force, the average of the three full bridge signals should be taken as the signal for the torque measurement. This can be demonstrated with a simple equation as shown in Equation (23), where γ_{torque} denotes the shear strain that is introduced purely by the torque, while $\gamma_{60°}$, $\gamma_{180°}$, and $\gamma_{300°}$ are

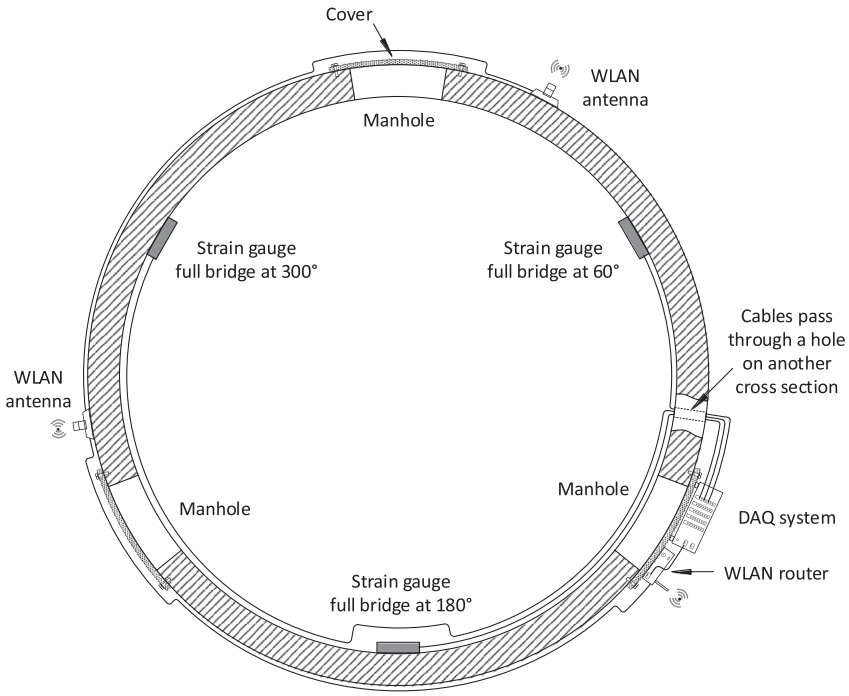

FIGURE 6 Cross section A-A on the intermediate shaft

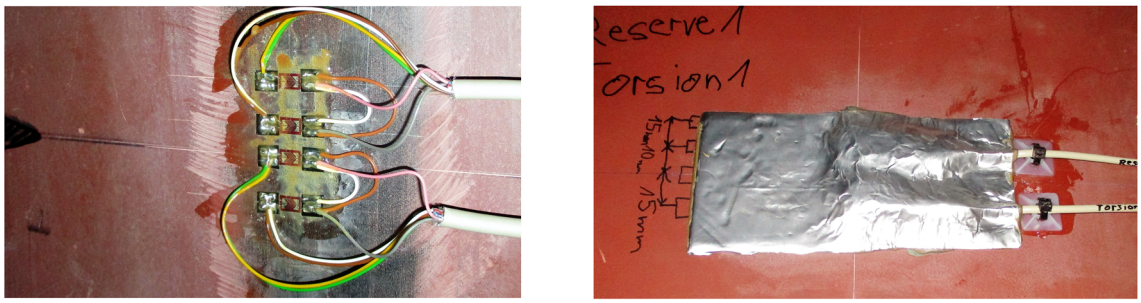

FIGURE 7 Examples of the strain gauges before and after the protective covering is affixed. At each position, two identical full bridges are used to provide redundancy. This explains why two output cables can be seen in each photo [Colour figure can be viewed at wileyonlinelibrary.com]

the corresponding local shear strains. Two photos showing how the strain gauge is mounted are presented in Figure 7.

$$\gamma_{torque} = (\gamma_{60^\circ} + \gamma_{180^\circ} + \gamma_{300^\circ})/3. \tag{23}$$

During the test, the manholes have to be closed with the covers. Therefore, the cables of the full bridge channels are led out through a small hole (available on another cross-section) to the data acquisition (DAQ) system, shown in Figure 6. The DAQ system is fixed to one of the manhole covers, with the help of the bolts for the cover. Since the strain gauges together with the DAQ system are located on the rotating part, a WLAN (Wireless LAN) connection is utilised for the communication between the rotating system and the stationary parts, including the data and time synchronisation server, as well as the remote measurement controller. Time synchronisation on the rotating DAQ system is realised through the WLAN connection in the network time protocol (NTP). The router of the WLAN system is also fixed to the cover. To ensure the quality of the wireless connection, three antennas are placed at equal separations along the circumference of the intermediate shaft.

In addition to the torque measurement, the speed and angular position are measured by an absolute encoder at the end of the test bench drive train. The encoder measures the rotation of the rear shaft relative to the adjacent bearing housing. This encoder is part of the test bench and has a resolution of 16384 CPR (counts per revolution). The signal is connected to a stationary DAQ system, with the same time reference as the rotating DAQ system.

To measure the electrical power, voltage and current sensors are installed on the input power cables of the two motors. A high sampling frequency DAQ system is used to measure the alternating voltage and current signals. The electrical power can be processed on the basis of the voltage and current measurements. The same source of time reference is also used in this system for the signal time stamps.

5.2 | Back-to-back test and torque calibration

Back-to-back tests are carried out following the method explained in Section 2. The electrical measurement of motor II is chosen as the reference during the test process. Since motor I is connected to a number of other components in the front, including the moment bearing of the load

TABLE 2 The whole test sequence for the torque calibration

Test Step	1	2	3	4	5	6	7	8	9	10
Motor II electrical power in relation to rated	20 %	40 %	60 %	75 %	85 %	20 %	40 %	60 %	75 %	85 %
Operating mode	A	A	A	A	A	B	B	B	B	B
Rotational speed, rpm	11	11	11	11	11	-11	-11	-11	-11	-11

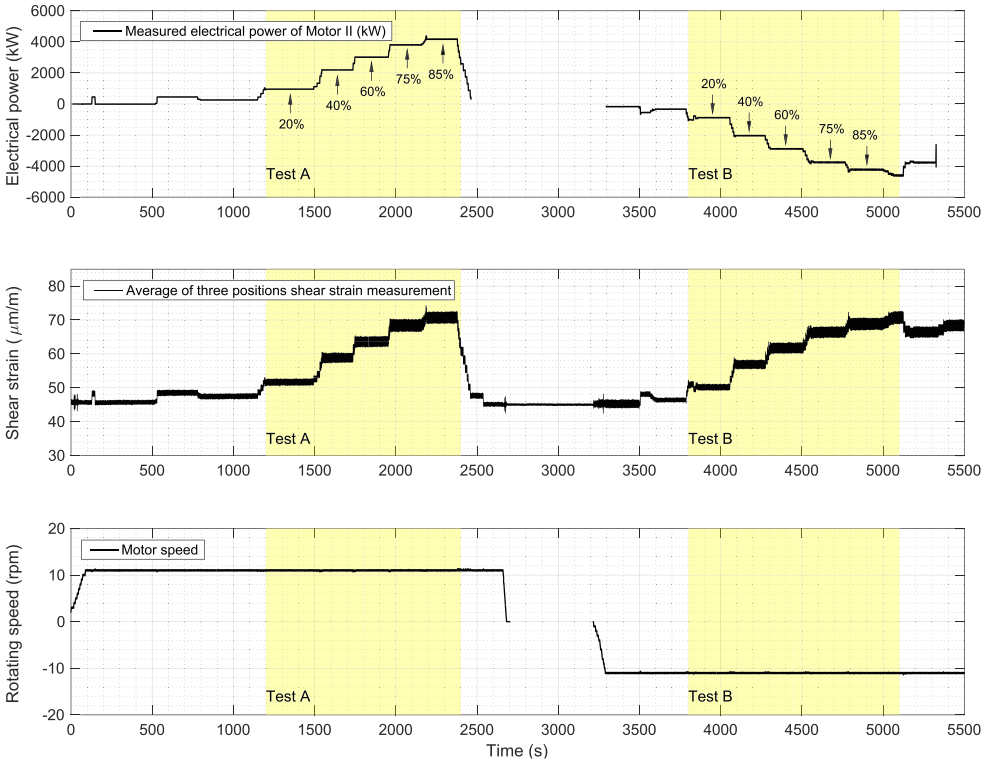

FIGURE 8 The measured raw signal of motor II electrical power (top), shear strain for the torque measurement (middle), and the rotational speed (bottom) [Colour figure can be viewed at wileyonlinelibrary.com]

application system, the friction loss is greater than motor II and will additionally increase the uncertainty in the calibration; therefore, the electrical measurement of motor II is preferred in the test and calibration process.

A test sequence of 10 steps is carried out with the motors run first in normal mode (test A), and later in reversed mode (test B). For each mode, the test is run in five different power levels. Motor II is taken as the reference, so that the electrical power of motor II is at a similar level in the corresponding steps of test A and test B. The test drive train rotates at the same speed, but in the opposite direction for the two modes. Detailed information about the test sequence is listed in Table 2. The values given in the table should be considered as the nominal. The actual values are controlled or tuned close to the nominal ones, and small discrepancies are allowed which deviate from the nominal values. Nevertheless, keeping the discrepancies as small as possible does help reduce the uncertainty in the calibration, especially the electrical power difference of motor II in mode A and mode B. Due to software limitations during the early phase of the commissioning, motor II is not run to 100 % of the rate power. The torque calibration is then calibrated in the range of 20 % to 85 % of the rated torque.

The raw data of the measured electrical power, the strain, and the rotational speed are shown in Figure 8, where the real time series of the complete test sequence are displayed. The segments corresponding to the test in mode A and mode B are highlighted in yellow in the figure. The system needs to come to a halt between the two operating modes because the drive train needs to change the direction of rotation. At the same time, the motor controllers also need to be reconfigured for the reversed operating mode. Although blank segments are seen in the signals of the electrical power and rotational speed, the test and the measurements are indeed carried out sequentially and continuously. Here, the speed signal is shown to provide a better indication of the operating condition, although the angle position instead of rotational speed is used in the calibration.

In Figure 8, the steps of different power levels can be clearly seen. For each step, the operation is kept on a stable state for at least 180 seconds, in order to have a stable measurement of sufficient length for the subsequent signal averaging. The power levels are marked on the plot of the electrical power. A positive electrical power stands for active power output (generator mode), while the negative power values indicate power input and that the machine is operating in motor mode. The motor speed stays at a very stable amplitude during both test A and test B. The rotating direction in test B can be seen to be opposite to the direction of test A. This ensures that the mechanical torque measured by the strain gauges is in the same direction for both test modes.

Before the torque calibration is possible, the k factor that describes the relationship between the power losses in the different operating modes as defined in Equation (2) must be estimated. In this test, the $\hat{k}$ factor is assumed to be 1.0 for all five test levels. Afterwards, the estimated $\tilde{X}$ and $\tilde{Y}$ can be obtained on each test level using the measured data as per Equation (12). From the same equation, it is possible to derive that $\tilde{X}$ has the

Power Level	I (20 %)	II (40 %)	III (60 %)	IV (75 %)	V (85 %)
$\tilde{X}$ (μm/m)	50.890	57.780	62.639	67.375	69.775
$\tilde{Y}$ ($kN \cdot m$)	796.9	1836.4	2563.1	3282.2	3645.4

TABLE 3 Estimated $\tilde{X}$ and $\tilde{Y}$ on different test levels

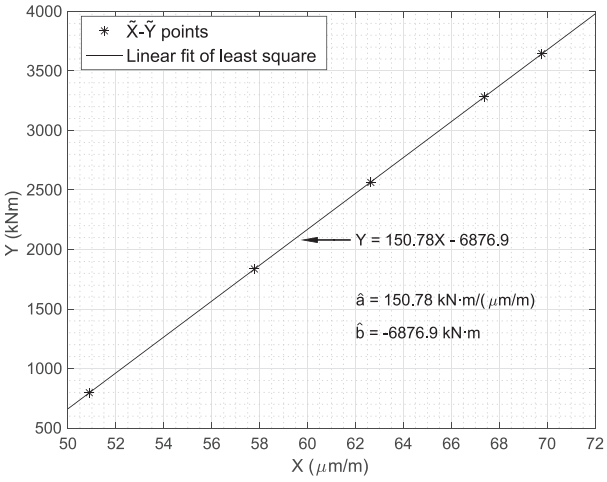

FIGURE 9 $\tilde{X}$ - $\tilde{Y}$ points and the linear fit with the least squares method

same unit as the raw measurement ε, a strain signal. The widely used unit micro-strain is adopted here as the unit of $\tilde{X}$ and expressed as $\mu m/m$ in accordance with the common practice in the industry. The $\tilde{Y}$ is the result of power divided by rotational speed and therefore has the dimension of torque. The unit $kN \cdot m$ is adopted here as the unit of $\tilde{Y}$. The values are listed in Table 3.

Each set of $\tilde{X}$ - $\tilde{Y}$ values in Table 3 can be plotted as one point in the X-Y plane. Five points corresponding to the five test levels can be drawn as shown in Figure 9. A linear fit of the five points is then possible. The slope and intercept of the line can be determined as $\hat{a} = 150.78\ kN \cdot m/(\mu m/m)$ and $\hat{b} = -6876.9\ kN \cdot m$, as per Equations (13) and (14). The calibrated torque measurement can be expressed as in Equation (24), with the unit of estimated torque $\hat{T}$ being $kN \cdot m$ and the unit of raw signal ε being $\mu m/m$.

$$\hat{T} = 150.78 \frac{kN \cdot m^2}{\mu m} \cdot \varepsilon - 6876.9\ kN \cdot m. \tag{24}$$

Unlike the conventional calibration methods that generate an accurate reference torque, the method described in this paper uses the electrical power as the reference and is based on the fact that the electrical power can be measured easily and with good accuracy. To present a better, visual explanation of the principle, the mean values of the mechanical, and electrical powers will be calculated and presented below. As the torque measurement is already calibrated and expressed in Equation (24), the average mechanical powers $\bar{\hat{P}}_{mech.A}$ and $\bar{\hat{P}}_{mech.B}$ on a certain test level can be expressed in Equation (25). The mean measured electrical powers $\bar{\tilde{P}}_{elec.A}$ and $\bar{\tilde{P}}_{elec.B}$ can easily be calculated in the normal way of averaging over the time domain.

$$\begin{cases} \bar{\hat{P}}_{mech.A} = \dfrac{\int_0^{\theta_A} \hat{T} d\theta}{t_A} \\ \bar{\hat{P}}_{mech.B} = \dfrac{\int_0^{\theta_B} \hat{T} d\theta}{t_B} \end{cases} \tag{25}$$

The mean mechanical and electrical powers $\bar{\hat{P}}_{mech.A}$, $\bar{\hat{P}}_{mech.B}$, $\bar{\tilde{P}}_{elec.A}$, and $\bar{\tilde{P}}_{elec.B}$ can be calculated for each of the five test levels listed in Table 3. For a better understanding, the values are plotted in Figure 10 together with level lines, similar to the procedure adopted in Figure 2. The plots for the five test levels are placed in turns along the horizontal axis according to the value of the nominal electrical power. The exact position along the horizontal axis is however not significant and therefore no grid or ticks are plotted on that axis. In contrast, the position along the vertical axis does have a concrete meaning and indicates the absolute value of test power.

From Figure 10, an equation linking the electrical power and the mechanical power can be obtained on each test level with the help of Equation (3). The calibration is therefore theoretically possible with two or more test levels. A potential improvement to the test process in this calibration can be seen in the figure. The electrical powers of motor II in the motor and generator modes can be tuned to be closer to each other, in order to have a lower uncertainty later on in the calibration. To achieve that, an on-line power analyser of the electrical measurement could be helpful.

5.3 | Uncertainty of the torque calibration

The uncertainty of the torque calibration comes mainly from the raw torque measurement, the electrical power, and the estimated k factor. Basic parameters used in the calculation are listed in Table 4. The notations of the error components are given in accordance with the definition in

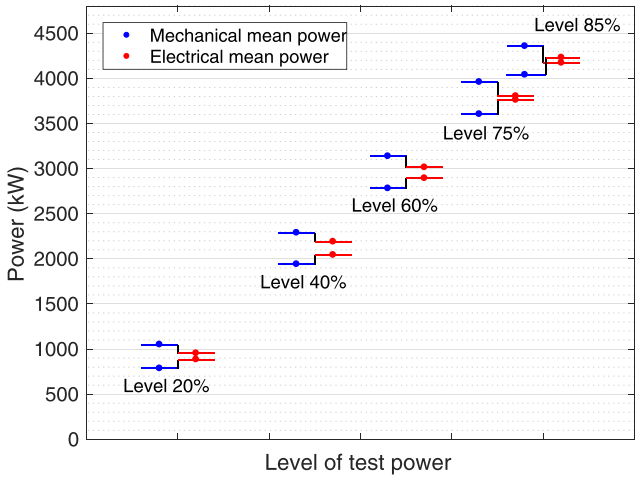

FIGURE 10 Mechanical mean power $\bar{\tilde{P}}_{mech.A}$, $\bar{\tilde{P}}_{mech.B}$ and electrical mean power $\bar{\tilde{P}}_{elec.A}$, $\bar{\tilde{P}}_{elec.B}$ of each test level displayed together [Colour figure can be viewed at wileyonlinelibrary.com]

TABLE 4 Basic uncertainty parameters related to the calibration

Uncertainty Component	Notation	Error Range	Standard Uncertainty u	Type
Sensitivity error of electrical power	c	±0.20 %	±0.12 %	Systematic
Offset error of electrical power	d	±3 kW	±1.73 kW	Systematic
Miscellaneous electrical power	Q	±2 kW	±1.15 kW	Random
Miscellaneous mechanical power	R	±8 kW	±4.62 kW	Random
Error of estimated $\hat{k}$ factor	δk	±20 %	±11.55 %	Systematic

TABLE 5 Standard uncertainty of $\tilde{X}$ and $\tilde{Y}$ at different torque levels

Standard Uncertainty	Unit	i=1	i=2	i=3	i=4	i=5
$\tilde{X}_i$ systematic	$\mu m/m$	0.0109	0.0144	0.0148	0.0148	0.0131
$\tilde{Y}_i$ systematic	$kN \cdot m$	1.8147	2.7568	3.4033	4.0856	4.4844
$-\tilde{Y}_i$ systematic due to c	$kN \cdot m$	0.9202	2.1205	2.9596	3.7899	4.2094
$-\tilde{Y}_i$ systematic due to d	$kN \cdot m$	1.5035	1.5035	1.5035	1.5035	1.5035
$-\tilde{Y}_i$ systematic due to δk	$kN \cdot m$	0.8623	1.8362	1.5007	0.5224	0.7227
$\tilde{X}_i$ random	$\mu m/m$	0	0	0	0	0
$\tilde{Y}_i$ random	$kN \cdot m$	0.8179	0.8179	0.8179	0.8179	0.8179

Section 3. All the uncertainty components shown in the table are assumed to obey the rectangular distribution[17] within the corresponding error range.

The electrical power measurement result from the three-phase voltage and current measurement, where high accuracy industrial sensors are used. The whole measurement chain is considered for the uncertainties of the voltage and current measurement channels, whereby the uncertainty of the sensors turns out not to play a major role. One of the important reasons is that the power factor of the motor is close to 1, which makes the otherwise very important phase error of the sensors less relevant to the overall power uncertainty. The miscellaneous errors of the electrical and mechanical powers Q and R are integrated over a period of time or angular rotation, as defined in Section 3. As mentioned in Section 5.2, the estimated factor $\hat{k}$ is adopted as 1 for all the five test levels. A uniform error of δk is also assumed for all the levels. Of course, both the estimated factor $\hat{k}$ and its error δk can be considered individually for each test level. Here, a uniform assumption is adopted for the sake of simplicity. As a result, a larger error range δk is also taken into consideration.

With the error parameters in Table 4 and according to the expressions for $\tilde{X}$ and $\tilde{Y}$ in Equations (9) and (10), the uncertainties of $\tilde{X}$ and $\tilde{Y}$ can be calculated as shown Table 5. The subscript i in the table denotes different test levels. The five levels from 20 % up to 85 % presented in Table 3 correspond to i being 1 to 5, respectively. In accordance with the discussion in Section 4.2, the systematic and random uncertainties are listed separately. Three contributions of the systematic uncertainty of $\tilde{Y}$ are also listed in the table. Note that the random uncertainties of $\tilde{X}$ are all zero, because the relevant uncertainties are attributed to the Y side, as shown in the definitions of the X and Y in Equations (9) and (10).

The correlation coefficient matrix $\boldsymbol{R}$ used in the calculation is presented in Table 6. The matrix $\boldsymbol{R}$ is defined in Section 4.2, and each of the entries represents the correlation coefficient between the corresponding standard systematic uncertainties. In Table 6, the corresponding standard systematic uncertainties are indexed in the first row and the first column. The values are taken with conservative considerations, and therefore, most of the entries are 1 or 0.

The estimated torque $\hat{T}$ is a function of the measured signal ϵ, with the estimated â and $\hat{b}$ as the sensitivity and offset parameters, shown in Equation (15). Therefore, the uncertainty of $\hat{T}$ comes from the uncertainties of â and $\hat{b}$, which are in turn dependent on the uncertainties of the $\tilde{X}$ and $\tilde{Y}$ values. Although by definition no uncertainty is attributed to the raw signal ϵ, it does exert an influence on the uncertainty of $\hat{T}$ by affecting and scaling the contribution of â. This influence is reflected in the partial derivatives of $\hat{T}$ with respect to $\tilde{X}$ and $\tilde{Y}$ in Equation (17). The partial derivatives have different values on different torque levels. An example is given in Table 7, where the measured raw signal ϵ equals 65 $\mu m/m$,

TABLE 6 The matrix of correlation coefficient $\boldsymbol{R}$

	$\sigma_{\tilde{X}_1}$	$\sigma_{\tilde{X}_2}$	$\sigma_{\tilde{X}_3}$	$\sigma_{\tilde{X}_4}$	$\sigma_{\tilde{X}_5}$	$\sigma_{\tilde{Y}_1}$	$\sigma_{\tilde{Y}_2}$	$\sigma_{\tilde{Y}_3}$	$\sigma_{\tilde{Y}_4}$	$\sigma_{\tilde{Y}_5}$
$\sigma_{\tilde{X}_1}$	1	1	1	1	1	0	0	0	0	0
$\sigma_{\tilde{X}_2}$	1	1	1	1	1	0	0	0	0	0
$\sigma_{\tilde{X}_3}$	1	1	1	1	1	0	0	0	0	0
$\sigma_{\tilde{X}_4}$	1	1	1	1	1	0	0	0	0	0
$\sigma_{\tilde{X}_5}$	1	1	1	1	1	0	0	0	0	0
$\sigma_{\tilde{Y}_1}$	0	0	0	0	0	1	0.92	0.86	0.79	0.73
$\sigma_{\tilde{Y}_2}$	0	0	0	0	0	0.92	1	0.98	0.94	0.88
$\sigma_{\tilde{Y}_3}$	0	0	0	0	0	0.86	0.98	1	0.98	0.95
$\sigma_{\tilde{Y}_4}$	0	0	0	0	0	0.79	0.94	0.98	1	0.99
$\sigma_{\tilde{Y}_5}$	0	0	0	0	0	0.73	0.88	0.95	0.99	1

TABLE 7 Partial derivatives of $\hat{T}$ with respect to the $\tilde{X}_i$ and $\tilde{Y}_i$ when $\varepsilon = 65\ \mu m/m$

Partial Derivative	Unit	i = 1	i = 2	i = 3	i = 4	i = 5	Sum
$\partial\hat{T}/\partial\tilde{X}_i$	$kN \cdot m/(\mu m/m)$	−6.776	−21.679	−32.282	−42.449	−47.615	−150.80
$\partial\hat{T}/\partial\tilde{Y}_i$	$kN \cdot m/(kN \cdot m)$	0.0450	0.1439	0.2136	0.2816	0.3160	1

Note. The values in the table are dependent on the torque level.

TABLE 8 Torque uncertainty owing to the calibration on several torque levels

Torque Level, $kN \cdot m$	Standard Uncertainty $u_{T.cal}$, $kN \cdot m$	Expanded Uncertainty U_{95}, $kN \cdot m$	U_{95} Relative to the Torque Level, %
1000	10.59	21.17	2.12
2000	10.90	21.79	1.09
3000	11.43	22.87	0.77
3600	11.85	23.71	0.66

corresponding to around 2920 $kN \cdot m$ of torque. Note that the summation of all the partial derivatives w.r.t. $\tilde{X}$ in the table is roughly equal to the inverse of the sensitivity â, while the summation of the partial derivatives w.r.t. $\tilde{Y}$ is exactly 1.

For the entire uncertainty of $\hat{T}$, the component $r(t)$ in Equation (15) also plays a role. It can be considered to be the uncertainty related to the signal quality. Again, since this paper focuses on the calibration method, only the uncertainty due to the calibration process will be analysed here. As defined in Section 4.2, the standard uncertainty of (15) caused by the calibration is denoted as $u_{T.cal}$. The expanded uncertainty with the 95 % confidence level is twice the value of $u_{T.cal}$, and is denoted as U_{95}. The uncertainty results of $\hat{T}$ due to the calibration on several torque levels are given in Table 8, where $u_{T.cal}$, U_{95} as well as the percentage of the U_{95} relative to the nominal torque are also presented.

It is seen in Table 8 that the uncertainty stays at a relatively stable level as the torque level increases. This is partly due to the conservative assumption made in Table 6 for the correlation coefficients. As the uncertainties $\sigma_{\tilde{X}_i}$ and $\sigma_{\tilde{X}_k}$ are assumed to be well correlated, this also means the $\tilde{X}$-$\tilde{Y}$ points in Figure 9 deviate more collectively from the true positions. Other reasons are the constant components that are not dependent on the torque level, for example, the offset error of the electrical power. Considering the percentage of the uncertainty (U_{95}) in relation to the measured torque, 0.66 % is achieved near the calibration upper limit around 3600 $kN \cdot m$. At lower torque levels, the percentage of uncertainty will be higher. However, for the majority of the measuring range, an uncertainty of less than 2 % of the nominal torque is achieved.

6 | DISCUSSION

The calibration process described in this paper focuses on the measurement and behaviour on the turbine side. Both the electrical and mechanical powers input and output of the the turbine are measured. In fact, the method can also be realised on the measurements on the test bench side with the electrical power of the test bench being measured. The method actually requires only two electrical machines that can both run in motor and generator modes and also in different directions. In this sense, the calibration method can also be used in other industries and applications where a similar test layout can be realised. One advantage of focusing on the test bench is that the properties of this object are stable regardless if a different turbine is under test. The disadvantage is the potentially greater uncertainty due to the large friction torque on the test bench.

The method can be carried out on turbines with or without a gearbox. As the turbine changes its operating mode and rotational speed at the same time in the reversed test mode, the gear teeth inside the gearbox always mesh on the same side. This eliminates the concern that the gearbox should not run under load in the opposite direction because the teeth are manufactured differently on the two sides. Nevertheless, it is recommended to consult the gearbox supplier regarding potential problems and the efficiency difference in the two test modes.

To increase the calibration accuracy, efforts should be taken on the whole measurement chains of all electrical and mechanical raw measurements. For the electrical power, special attention should be paid to the time delay and hence the phase errors between the voltage and the current signals. For the torque measurement, the signal drift resulting from temperature change and creep has a direct impact on the calibration results. Furthermore, a proper time-synchronisation is imperative, in order to avoid time and phase shift between different signal channels.

For the test process, several efforts can be taken in the preparation and during the test. First, a preheating prior to the calibration test process is necessary in order to reach a relatively stable temperature and lubrication status for the whole drive train and the measurement system. Second, the ambient temperature should be kept as stable as possible during the whole test process, so that temperature changes in all systems are kept under control. Third, the electrical power input and output amplitudes should be kept as close to each other as possible. In the case shown in Figure 10, further improvement could be achieved by better controlling the electrical powers to be at the same level. Another effort is to try to have the power factor of the electrical machine as close to 1 as possible, which helps reduce the uncertainty in the electrical power.

The biggest contribution to the uncertainty for the calibration is in many cases the uncertainty in the assumed $\hat{k}$ factor. As the k factor cannot realistically be determined by a test, it must be chosen either with the help of detailed analysis of the drive train and the electrical machine or with an approximate assumption which results in a large uncertainty. Therefore, for a smaller uncertainty of the $\hat{k}$ factor, a detailed analysis of the power loss and the efficiency of the drive train is necessary.

7 | CONCLUSIONS

The proposed new calibration method takes advantage of the high accuracy of the electrical power measurement while at the same time it greatly reduces the uncertainty introduced by the power losses in the drive train. Based on the fact that the drive train tends to have a similar power loss in both motor and generator mode, the effect of the power loss can be largely compensated by carrying out the test in both the normal mode and in the reversed mode. With measured data from both test modes, an equilibrium can be drawn between the electrical and mechanical powers. The calibration can be carried out with the help of several such equilibriums on different torque levels.

No special instrumentation is needed for the method. All the sensors and equipment used in the calibration are produced in series and commercially available. The necessary test process can be carried out with the same mechanical layout as the normal test, which means that no additional structural reconfigurations or logistical effort is necessary. As a result, the calibration is low cost and time efficient. It can also be easily repeated whenever necessary.

One prerequisite of the calibration method is the ability of the test bench and the DUT (device under test) to run in reversed mode and operate in both directions up to the rated power. The calibration method is demonstrated on a torque measurement between two 5-MW driving motors of a nacelle test bench for the wind turbine, where both the calibration parameters and the accompanying uncertainties are determined. With conservative considerations, the uncertainty due to calibration is, in this case, within 0.7 % at upper limit of the calibration range. Better calibration accuracy can be achieved by reducing the electrical power uncertainty, improving the quality of the raw torque-measuring signal, and most importantly, by a better analysis of the drive train and therefore a smaller uncertainty in the k factor estimation.

ORCID

Hongkun Zhang https://orcid.org/0000-0001-5172-4867
Jan Wenske https://orcid.org/0000-0001-7035-1947
Mohsen Neshati https://orcid.org/0000-0001-6701-0666

REFERENCES

1. Schlegel C, Kahmann H, Kumme R. MN·m torque calibration for nacelle test benches using transfer standards. *ACTA IMEKO*. 2016;5(4):12-18.
2. DIN 51309:2005-12, Materials testing machines — Calibration of static torque measuring devices.
3. Kahmann H, Schlegel C, Kumme R, Röske D. Principle and design of a 5MNm torque standard machine. In: *IMEKO TC3, TC5 and TC22 International Conference 2017*; 2017.
4. Weidinger P, Foyer G, Kock S, Gnauert J, Kumme R. Development of a torque calibration procedure under rotation for nacelle test benches. *J Phys Conf Ser*. 2018;1037(5):052030–052039. https://doi.org/10.1088/1742-6596/1037/5/052030
5. Weidinger P, Schlegel C, Foyer G, Kumme R. *Characterisation of a 5 MN·m torque transducer by combining traditional calibration and finite element method simulations*. In: *AMA Conferences*; 2017.
6. Foyer G, Kock S. Measurement uncertainty evaluation of torque measurements in nacelle test benches. In: *23rd IMEKO TC3, 13th TC5 and 4th TC22: International Conference, TC3, TC5 and TC22 International Conference*; 2017.
7. Peschel D, Mauersberger D, Schwind D, Kolwinski U. The new 1.1 MNm torque standard machine of the PTB Braunschweig/Germany. In: *19th IMEKO TC3: TC3 International Conference on Force, Mass and Torque, TC3 International Conference on Force, Mass and Torque, Cairo, Egypt*; 2005:19-25.
8. Kock S, Jacobs G, Bosse D, Sharma A. Friction as a major uncertainty factor on torque measurement in wind turbine test benches. *J Phys Conf Ser*. 2018;1037(6):062001–062008. https://doi.org/10.1088/1742-6596/1037/6/062001
9. Averous NR, Stieneker M, Kock S, et al. Development of a 4 MW full-size wind-turbine test bench. In: *2015 IEEE 6th International Symposium on Power Electronics for Distributed Generation Systems (PEDG)*:1-8; 2015. https://doi.org/10.1109/PEDG.2015.7223108.
10. Zhang H, Neshati M. An effective method of determining the drive-train effciency of wind turbines with high accuracy. *J Phys Conf Ser*. 2018;1037(5):052013–052023. https://doi.org/10.1088/1742-6596/1037/5/052013
11. Zhang H, Eich N, Pilas M, Wenske J. Verfahren zum Ermitteln einer Effizienz und/oder zum Kalibrieren eines Drehmoments eines Antriebsstrangs, insbesondere einer Windenergieanlage. Patent DE102018203525 (in German); 2019.
12. Coleman HW, Steele WG. *Experimentation, validation, and uncertainty analysis for engineers*. 4th ed. Wiley; 2018.

13. Errors due to Wheatstone bridge nonlinearity. Tech Note TN-507-1: Vishay Precision Group; 2010. http://www.vishaypg.com/doc?11057.
14. Schäck MM. High-precision measurement of strain gauge transducers at the physical limit without any calibration interruptions. In: *IMEKO-TC3 International Conference*. Cape Town, South Africa; 2014.
15. Plane-shear measurement with strain gages. Tech Note TN-512-1: Vishay Precision Group; 2010. http://www.vishaypg.com/docs/11062/tn5121tn.pdf.
16. Zhang H, Ortiz de Luna R, Pilas M, Wenske J. A study of mechanical torque measurement on the wind turbine drive train — ways and feasibilities. *Wind Energy*. 2018;21(12):1406-1422. https://doi.org/10.1002/we.2263
17. Evaluation of measurement data — Guide to the expression of uncertainty in measurement (GUM 2008). JCGM - Joint Committee for Guides in Metrology; 2008.
18. *Web page DyNaLab, Nacelle Testing and Examination of Electrical Characteristics.* : Frauhofer IWES; https://www.iwes.fraunhofer.de/en/test-centers-and-measurements/nacelle%-testing-and-certification-of-electrical-characteristics. Accessed October 2018.

How to cite this article: Zhang H, Wenske J, Reuter A, Neshati M. Proposals for a practical calibration method for mechanical torque measurement on the wind turbine drive train under test on a test bench. *Wind Energy*. 2020;23:1048–1062. https://doi.org/10.1002/we.2472